

pubs.acs.org/JPCC Article

Interfacial Electric Fields Drive Rearrangement of Adsorbed Cysteine and Electrolyte Ions on Au Electrodes

Hari R. Sudhakar, Julie N. Renner, and Robert E. Warburton*



Cite This: J. Phys. Chem. C 2024, 128, 18063-18073



Read Online

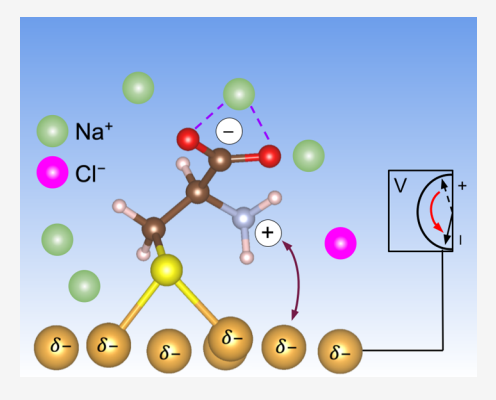
ACCESS I

Metrics & More

Article Recommendations

Supporting Information

ABSTRACT: Electrode surfaces modified with peptides or other biomolecules are of great interest for applications in catalysis and separations. At the electrochemical interface, the structure of biomolecular adsorbates may be sensitive to the applied potential and the distribution of solvent and ions near the electrode surface. Herein, periodic density functional theory (DFT) calculations are used to describe changes in the adsorption structure of the L-cysteine amino acid on Au(111) as a function of applied potential. This theoretical study reveals the fundamental mechanisms of potential-dependent rearrangement of cysteine on electrode surfaces. These systems are analyzed using a hybrid quantum—classical computational approach that combines constant-potential periodic DFT with a classical representation of the liquid electrolyte. In agreement with experimental measurements, grand canonical thermodynamic analyses suggest that the cysteine exists primarily in its zwitterionic form over a wide range of applied potentials. The structure of adsorbed zwitterionic cysteine is dictated by the cationic ammonium and anionic carboxylate functional



groups, where these charged moieties experience competing Coulombic interactions with the charged Au(111) surface and the electrolyte ions within the electric double layer. These competing interactions drive the rearrangement of cysteine with applied potential, which in turn determines the nature of ion structuring at the interface. The potential-dependent free energies of cysteine zwitterions are also significantly influenced by the ionic strength of the electrolyte because of the interactions between charged zwitterion functional groups and oppositely charged electrolyte ions. Understanding the interplay between adsorption structure, applied potential, and electrolyte ion structuring can guide the assembly of structured biomolecules on solid surfaces. The impact of zwitterionic amino acids and peptides on near-surface electrolyte composition may be further exploited to tailor microenvironments for various applications of interfacial electrochemistry.

■ INTRODUCTION

Peptide-based monolayers on metal surfaces are a promising class of bioinorganic interfaces that can be used for applications in catalysis, drug delivery, sensing, and separations.^{1–9} The wide variety of applications in which peptide-functionalized interfaces may be found implies a diverse array of chemical environments that could impact the properties of peptides on solid surfaces. At electrochemical interfaces, for example, applied potential and electrolyte ionic strength influence peptide structure on metal electrodes.^{10,11} Yet, a molecular-level understanding of such electrolyte and potential effects on the structure and properties of bioinorganic interfaces is limited. Thus, the prediction of the chemical structure of surface-conjugated amino acids and peptides under complex electrochemical environments requires theoretical modeling approaches that account for the effects of solvent, ions, and interfacial electric fields.

To understand more complex polypeptide structure on solid surfaces, it is essential to first describe the adsorption behavior of adsorbed amino acids under different chemical environments. The amino acid cysteine is commonly used as a linker to conjugate peptides to metal surfaces because it has a thiol headgroup that enables the formation of strong metal—sulfur

bonds on solid surfaces. ^{12–17} Cysteine can exist in either neutral, zwitterionic, anionic, or cationic forms; however, cysteine is typically a zwitterion at biological pH. ¹⁸ Compared to neutral cysteine which has no formally charged functional groups (Figure 1A), zwitterionic cysteine contains both cationic ammonium (NH₃⁺) and anionic carboxylate (COO⁻) functional groups (Figure 1B). Although the cysteine zwitterion is also charge neutral, we use the notation "neutral" to specifically refer to the form that does not have formally charged functional groups. Several theoretical and experimental studies have characterized the properties of L-cysteine adsorbed on gold surfaces, demonstrating adsorption occurs through sulfur at moderate pH. ^{19–26} Reflection anisotropy and surface-enhanced Raman spectroscopy studies have shown that L-cysteine

Received: June 25, 2024
Revised: September 26, 2024
Accepted: September 27, 2024
Published: October 10, 2024





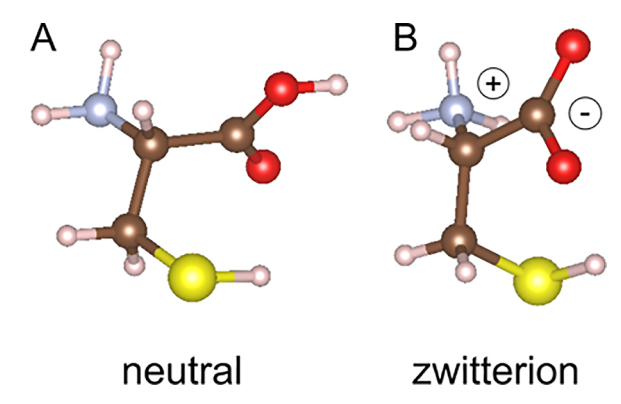


Figure 1. (A) Neutral and (B) zwitterionic forms of L-cysteine considered for the calculations in this work. S, O, C, N, and H atoms are shown in yellow, red, brown, blue, and white, respectively.

undergoes conformational changes with applied electric field when adsorbed to metal electrodes. 19,20 In one of these studies, it was shown that the carboxylate group orients toward the surface at positive potentials.²⁰ Multiple experimental studies have shown that cysteine primarily exists as a zwitterion when adsorbed to metal surfaces in aqueous electrolytes. 20,23-25,27 Yet, analogous theoretical modeling studies have focused on neutral cysteine because these simulations have been performed in vacuum, which cannot stabilize the charged zwitterion.^{21,22} Moreover, the effects of applied potential on adsorbateelectrolyte interactions and the chemical state of L-cysteine (neutral or zwitterionic) has not been investigated computationally. The applied potential and the associated interfacial electric field can significantly impact the structure, energetics, and reactivity of adsorbates on solid surfaces. ²⁸⁻³⁴ Because the chemical state of cysteine can impact adsorption strength, 35 such structural predictions are critical to understanding and controlling the properties of biomolecular adsorbates on solid surfaces.

Herein, periodic density functional theory calculations (DFT) with the effective screening medium and reference interaction site model (ESM-RISM) are used to model the chemical structure of adsorbed cysteine on Au(111) under applied potential and in the presence of electrolyte ions. 36,37 Cysteine and Au(111) are modeled with DFT, whereas the electrolyte is modeled classically using the RISM approach. Charged surface calculations are enabled by the ESM, where the fictitious charged particle (FCP) method allows for charge fluctuations and constant Fermi level calculations consistent with the electronically grand canonical ensemble. This theoretical approach enables a systematic study into the effects of applied potential and electrolyte ions on the structure of adsorbed cysteine, which in turn can affect electrolyte ion structuring at the interface. Specifically, we have focused on the how applied potential impacts the orientation of cysteine on the surface, as well as energetics of the different chemical states of cysteine (i.e., neutral or zwitterion). Because the applied potential changes the structure of the electrolyte near the interface, charged functional groups have Coulombic interactions with both the charged electrode surface and the electrolyte ions. Tailoring the structure of bioinorganic interfaces in electrochemical environments can be used to advance molecular-level understanding of biomolecules on solid surfaces, allowing for further development of applied functional materials.

METHODS

Periodic DFT calculations were conducted using the Quantum ESPRESSO code. The PBE exchange—correlation functional with Grimme's D3 dispersion correction (PBE-D3)^{40,41} was used for all calculations. We used PBE-D3 to account for dispersion forces associated with the hydrogen bonding interactions between the components of the cysteine zwitterion. The atomic cores were modeled using projector-augmented wave (PAW) pseudopotentials from pslibrary. 42,43 The valence states were expanded in a plane-wave basis set with kinetic energy and charge density cutoffs of 60 and 360 Ry, respectively. We employed Methfessel-Paxton smearing of the electronic states with a smearing width of 0.01 Ry. We modeled the adsorption of cysteine (neutral and zwitterion) to a four-layer 3 × 3 Au(111) slab, where the bottom two layers were fixed to their bulk positions. The Brillouin zone was sampled using 4×4 \times 1 Monkhorst—Pack k-point mesh. The system was placed in a cell with sufficient distance between periodic images in the direction normal to the slab (\sim 15 Å). The geometry of the structures were optimized with a force criterion of 0.002 Ry/

The effects of applied potential and implicit solvation were accounted for using the ESM-RISM method, which has been implemented in Quantum ESPRESSO by Otani and coworkers. 36,37 The ESM-RISM method has been shown to give accurate representations of solvation energies and electrode—electrolyte interfacial properties. 44-46 Here, we have chosen to use such an implicit electrolyte model, ⁴⁷ rather than a full atomistic representation of the electrolyte. ^{48,49} While a fully atomistic model may provide a more accurate representation of the interactions between the electrode and the electrolyte, the ESM-RISM model enables calculations to be performed in a thermodynamic ensemble that is open to both electrons and their corresponding countercharge species in the electrolyte. We note that in contrast to a Poisson-Boltzmann model of the electrolyte, the solvent and ions in the RISM electrolyte model are represented using geometries, partial charges, and force-field parameters, making the implicit electrolyte sensitive to the local chemical and electrostatic environment. 36,37,50 In this hybrid quantum—classical modeling approach, the atomic system (i.e., the solute) is treated using DFT whereas the solvent molecules and electrolyte ions are treated classically using the RISM implicit solvation. Any net charge on the solute is compensated by an equal and opposite electrolyte charge to maintain charge neutrality with the vacuum/slab/solvent ESM boundary conditions. 36,51,52 A 160 Ry kinetic energy cutoff for the solvent correlation functions was employed. The solvation free energies were computed using the Kovalenko-Hirata closure relation along with the Gaussian fluctuation correction.⁵³ The Laue-RISM method³⁷ was used to set the electrolyte region in an expanded unit cell of length 73 Å. For more dilute electrolyte concentrations (<0.1 M), an expanded unit cell of length 284 Å was used to ensure that the counter charge goes to zero at the cell boundary. The aqueous electrolyte contained Na+ and Cl- ions and was modeled with the RISM method using Dang's three-site polarizable water model while the water molecules were described using the simple point charge (SPC) model of water. 54-56 Previous RISM studies using the SPC water model have demonstrated accurate radial distribution functions as well as hydration free energies when compared to experiment.⁴⁶ Furthermore, the atomic density distributions in RISM can capture the redistribution and

reorientation of solvent and ions with applied potential (Supporting Information, Figures S6B and S8). The solute–electrolyte interactions were accounted for using the Lennard–Jones parameters from the Universal force field model.⁵⁷

The fictitious charged particle (FCP) method is used to control the Fermi energy (i.e., the computational electrode potential) in the DFT/ESM–RISM calculations. ⁵⁸ In this approach, a target Fermi level is specified as an input. The FCP iterations are performed after each self-consistent field iteration, where the FCP method adjusts the system charge to ensure convergence to the target Fermi level within a 0.01 eV convergence threshold. In this approach, the electronic grand potential (Ω) is calculated as

$$\Omega(\mu_{\rm e}) = A - \Delta n_{\rm e} \mu_{\rm e} \tag{1}$$

where A is the Hemholtz free energy, $\Delta n_{\rm e}$ is the excess number of electrons, and $\mu_{\rm e}$ is the chemical potential of the electrons. Note that $\mu_{\rm e}=-\varepsilon_{\rm F}$, where $\varepsilon_{\rm F}$ is the Fermi energy relative to the bulk RISM electolyte electrostatic potential energy. In the present study, the calculations of A do not include zero point and entropic effects and we therefore assume A to be approximately equal to the DFT energy. We made this approximation because we assume that the zero point energy (ZPE) and entropic terms will cancel when comparing relative energetics between systems with same stoichiometry. We note that differences in ZPE and vibrational entropy could become more significant at very negative or very positive potentials where the vibrational energy levels of polar bonds may be sensitive to the local electric field via the vibrational Stark effect. S9-65 Yet, we expect these changes in ZPE and TS to be small and systematic for the phases studied herein.

■ RESULTS AND DISCUSSION

We first analyzed the adsorption configurations of cysteine on Au(111) in vacuum. Because previous theoretical and experimental studies have shown that the adsorption occurs by thiolate bond dissociation and Au-S bond formation, 22-24,26,63,64,66,67 we considered different adsorption configurations involving Au-S bond formation on the Au(111) surface (Figure S1). We considered adsorption to different surface sites (i.e., top, bridge, and hollow sites), as well as different configurations as defined by bond angles of cysteine, informed by previous studies of this system in vacuum. ^{21,22} Initial configurations were generated by specifying adsorption sites and bond angles in the Atomic Simulation Environment. 68 Note that more high-throughput automated tools may be needed to exhaustively enumerate over possible adsorption configurations of more flexible adsorbates (e.g., longer biomolecules such as polypeptides). 69,70 Further details are provided in the Supporting Information, Section S1. Starting from these different cysteine configurations, we performed geometry optimizations to sample the energetics of various local minima. The different local minima can be viewed as analogous to energetically feasible dihedral angles represented in Ramachandran plots of amino acid residues in proteins.⁷¹ All geometry optimizations in vacuum converged to the neutral cysteine configuration; we did not identify a local minimum for zwitterionic cysteine in vacuum. Although the present study focuses on low-coverage models, we note that the zwitterion could also be stabilized by intermolecular hydrogen bonding at high coverages. 72,73 In vacuum, the most energetically favorable cysteine adsorption configuration is to the bridge site with a tilt

angle of 58° and adsorption energy of -0.82 eV. The tilt angle is defined as the angle between the S–C bond and the surface normal. The bridge (br) site has also been identified as the most thermodynamically favorable adsorption site for thiols on Au(111). 21,22,24,26,66,74,75 We also identified a metastable cysteine adsorption structure to the fcc site with a tilt angle of 3.1° and adsorption energy of -0.65 eV (Table S1). The tilt angles and adsorption energies for these two most stable configurations are in close quantitative agreement with previous DFT studies of cysteine adsorption on Au(111), as shown in the Supporting Information, Table S1. 21,74

To account for solvent and ion effects on the adsorption configuration of cysteine, the electrolyte is modeled classically using the ESM–RISM method, which is described further in the Methods section. The ESM–RISM approach has been applied in previous studies to predict potential-dependent adsorption configurations and surface thermodynamics. The ESM–RISM calculations were performed using 1 M NaCl in water as the classical implicit electrolyte, where any charge on the solute is compensated by the electrolyte ions. Figure 2 shows a subset

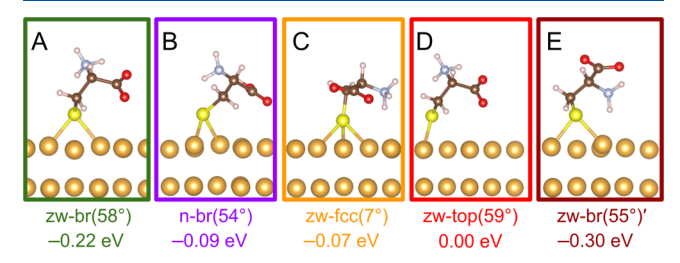


Figure 2. Optimized geometries and grand potentials at zero total charge in 1 M NaCl electrolyte) for zwitterionic (zw) and neutral (n) cysteine, adsorbed at different tilt angles to the Au(111) surface (given in parentheses). Yellow, red, brown, blue and white represent S, O, C, and H atoms, respectively. Br (bridge), fcc, and top denote the different adsorption sites on Au(111). The ' in zw-br(55°)' notation denotes that the NH₃+ functional group is oriented toward the surface, as opposed to the zw-br(58°) structure where the COO⁻ functional group is oriented toward the surface. Other optimized geometries obtained are shown in the Supporting Information, Figure S2. By construction, Ω is taken to be zero for the zw-top(59°) at zero total charge.

of the neutral (n) and zwitterion (zw) adsorption configurations that were analyzed: zw-br(58°), zw-fcc(7°), zw-br(55°)′, zw-top(59°) and n-br(57°). Figure 2 also shows the corresponding grand potentials Ω calculated at zero total charge (i.e., the potential of zero free charge). The free energy of the zw-top(59°) configuration at zero total charge is taken to be zero by construction. The notation for these adsorption configurations denotes the form of adsorbed cysteine (neutral or zwitterion), the adsorption site (top, br, or fcc), and the tilt angle. Additionally, to distinguish the configurations in the bridge site, the zw-br(55°)′ configuration is accompanied by a prime symbol (′) to denote that its NH $_3^+$ functional group is oriented toward the surface. Additional configurations were also analyzed, and these structures are shown in the Supporting Information, Figure S2.

To understand the effect of applied potential on the stability of these different configurations, we calculated the grand potentials of different adsorbed cysteine configurations on Au(111) at different applied potentials (Figure 3). All electrode potentials are presented relative to the potential of zero charge (PZC) of the clean Au(111) slab in aqueous electrolyte containing 1 M NaCl, and are thus denoted $U - U_{PZC}$. The

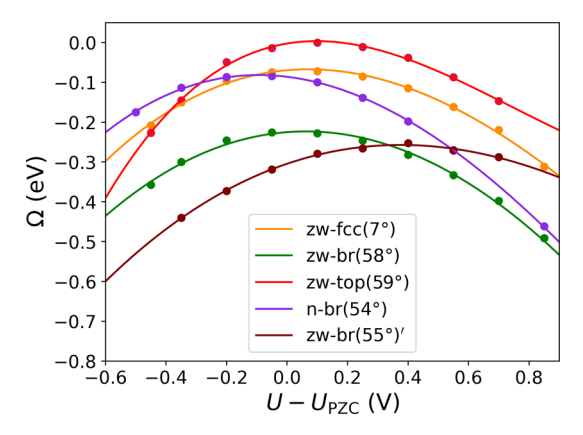


Figure 3. Grand potential (Ω) of adsorbed cysteine configurations as a function of applied potential $(U-U_{\rm PZC})$ in water with 1 M NaCl. The grand potentials were calculated relative to the grand potential of the zw-top(59°) configuration (red) calculated at zero total charge. The points marked by filled circles indicate the energies obtained from the DFT/ESM-RISM calculations. The solid lines are a cubic polynomial fit to the computed data. Further discussion about the cubic polynomial fits is given in Section S2 of the Supporting Information.

 $U_{\rm PZC}$ reference is calculated for a Au(111) slab with zero total charge. This value is chosen as a common absolute reference potential even though each configuration has a different potential of zero free charge, ⁸¹ as suggested by the free energy maxima at different values of $U - U_{PZC}$ for each configuration. 82-85 The different potentials of zero free charge can be attributed in part to the different dipole moments of the cysteine configurations considered. 86,87 The effect of the dipole moment perpendicular to the surface for these optimized configurations in vacuum is discussed in the Supporting Information, Section S4. The relative electrode potential is therefore calculated as U – $U_{\rm PZC}$ = $-(\mu_{\rm e}-\mu_{\rm e,PZC})/e$, where e is the electronic charge. This approach was used to calculate the grand potential Ω as a function of electrode potential for the different cysteine configurations shown in Figure 2. The data in Figure 3 are fit to a cubic polynomial as has been done in previous work.⁷⁸ As also observed in previous work, 82 a quadratic polynomial fits the data well near the potential of zero free charge (i.e., the maximum of the free energy curve), and the cubic terms are only necessary to fit the data at very high or low potentials (Supporting Information, Figure S4).

The subset of configurations shown in Figure 3 represent the most stable binding configurations of the cysteine zwitterion at each adsorption site, in addition to the most stable adsorption configuration of neutral cysteine. The results in Figure 3 demonstrate that over the range of potentials studied, the zwbr(58°) and zw-br(55°)' configuration have the lowest free energy for the potential ranges considered. Notably, the zwbr(58°) configuration has the lowest free energy at positive potentials, whereas the zw-br(55)' configuration has the lowest free energy at negative potentials. The zw-br(58°) and zwbr(55)' adsorption configurations have the same adsorption site (br) and similar tilt angles to the low-energy adsorption configuration of neutral cysteine in vacuum as calculated in the present work (Supporting Information, Table S1) and in previous studies.²¹ The prediction of a similar adsorption geometry to that which was obtained in vacuum suggests that the low-energy adsorption geometries obtained using the ESM-RISM method are chemically reasonable. Although the adsorption studies in vacuum show that cysteine exists in its

neutral form, the ESM–RISM results in Figure 3 are in agreement with various experimental studies that show cysteine is a zwitterion in aqueous electrolytes. ^{26,27,66,67} Furthermore, these results are also consistent with previous studies showing that thiols preferentially adsorb to bridge sites on close packed metal surfaces. ⁷⁴ The grand potentials of the other configurations studied are shown in the Supporting Information, Figure S3.

The thermodynamic information in Figure 3 can be used to determine the relative population (pop_i) of given cysteine configuration i as a function of applied potential. Figure 4 shows

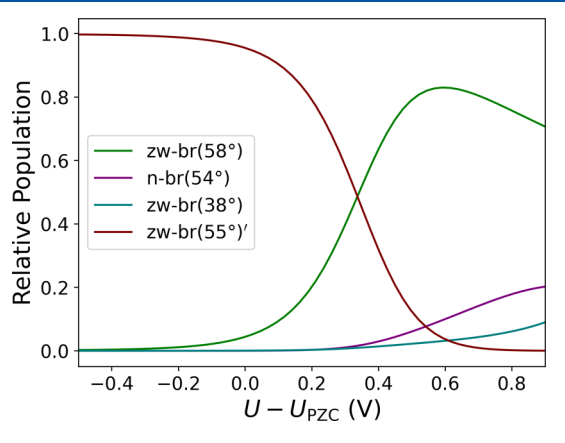


Figure 4. Relative population of adsorbed cysteine configurations as a function of applied potential $(U-U_{\rm PZC})$ in water with 1 M NaCl. These data are shown only for configurations with significant coverage. The zw-br(38°) structure is shown in the Supporting Information, Figure S2.

how the relative populations of different adsorbed cysteine configurations vary with applied potential. Note that these relative populations do not represent the surface coverage of cysteine, but rather the probability that an adsorbed molecule adopts a given configuration. As such, the relative population of a given cysteine configuration i was calculated from a Boltzmann distribution:

$$pop_{i} = \frac{exp\left(\frac{-\Omega_{i}}{kT}\right)}{\sum_{j} exp\left(\frac{-\Omega_{j}}{kT}\right)}$$
(2)

where the sum in the denominator is taken over all configurations studied. Configurations with negligible relative populations over the range of potentials studied are not included in Figure 4 for clarity. As the grand potential calculations in Figure 3 suggest, Figure 4 also shows that zw-br(58°) is the dominant configuration at potentials positive of ~ 0.33 V, whereas zw-br(55°)' is the dominant configuration at potentials negative of ~ 0.33 V. At a potential of ~ 0.9 V, however, the calculated equilibrium populations suggest that about 20% of the adsorbed cysteines will adsorb in the neutral form in the n-br(54°) configuration. The results at high potentials align with experimental studies that showed an adsorbed monolayer of cysteine composed of zwitterions ($\sim 76\%$) and neutral ($\sim 24\%$) cysteine.

Although the zw-br(58°) and zw-br(55°)' configurations are the most thermodynamically stable for the range of potentials studied, the free energies of the other adsorbed cysteine configurations each exhibit distinct potential dependencies. For example, the free energy of the neutral n-br(54°) structure is

high relative to other configurations at negative potentials; however, it is nearly degenerate to the low-energy zw-br(58°) configuration at more positive potentials. This trend is also reflected in Figure 4, which shows an appreciable population of neutral cysteine adsorbed to the surface at positive potentials. Overall, Figure 3 shows that applied potential has a significant impact on the relative free energies of the different adsorption configurations, especially at negative potentials where many of the free energy curves intersect.

Because the zw-br(58°) and zw-br(55°)' configurations are thermodynamically favored at positive and negative potentials, respectively, the potential-dependent thermodynamic predictions in Figures 3 and 4 suggest that the applied potential can drive reorientation of adsorbed cysteine on the electrode surface. We hypothesize that the underlying mechanism is the potential-dependence of the Coulombic attraction/repulsion between the charged moieties of the zwitterion and the electrode surface. These electrostatic interactions are depicted by the schematic in Figure 5. At more negative potentials, the electrode

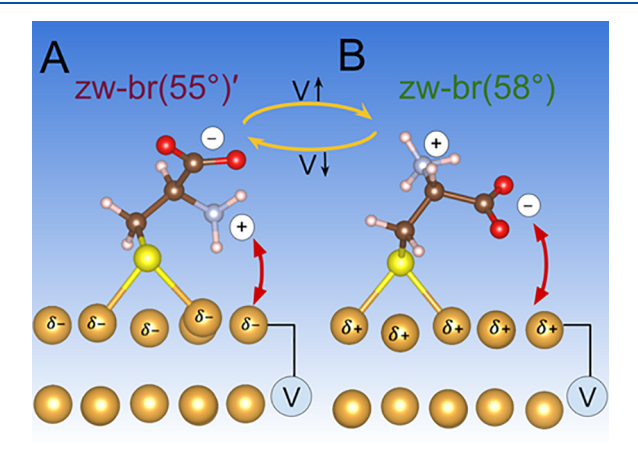


Figure 5. Schematic of the electrostatic interactions between the charged NH₃⁺ and COO⁻ moieties of zwitterionic cysteine and the charged Au surface. Coloumbic interactions between these functional groups of different charges are hypothesized to drive the potential-dependent reorientation of cysteine that is suggested by thermodynamic analysis.

surface adopts a negative surface charge stabilizing zwitterionic configurations with the NH $_3^+$ functional group oriented toward the surface (i.e., the zw-br(55°)′ configuration in Figure 5A). At positive potentials, the electrode is positively charged and cysteine is stabilized by the COO $^-$ functional group being oriented toward the surface (i.e., the zw-br(58°) configuration in Figure 5B). These results are in qualtiative agreement with experimental studies of cysteine on gold, which demonstrate the same general trend.

The electrostatic interactions between cysteine and the electrode surface can justify the reorientation of zwitterions relative to the surface; however, such surface—cysteine interactions cannot explain some of the other thermodynamic trends in Figures 3 and 4. Because the zw-br(58°) configuration contains a negatively charged carboxylate group oriented toward the surface (Figure 2A), for example, it is reasonable to expect that this structure would be higher in free energy than the n-br(54°) configuration at more negative potentials when the Au surface is also more negatively charged.²⁰ Instead, the data show that zw-br(58°) has a lower free energy than its n-br(54°) neutral analogue at negative applied potentials. These trends

imply that other effects beyond Coulombic repulsion between the Au surface and the charged functional groups of zwitterionic cysteine impact the potential-dependent adsorption thermodynamics.

To elucidate possible chemical mechanisms beyond surface—cysteine electrostatics that may underly the potential-dependent thermodynamic trends, we examined the ensemble-averaged concentration profiles of different species in the classical electrolyte determined from the ESM–RISM calculations. Ions distribute within the electric double layer at the electrode—electrolyte interface to maintain local charge neutrality. In the case of adsorbed cysteine, however, electrolyte structuring in the double layer can also be influenced by the charged COO⁻ and NH⁺₃ functional groups of the cysteine zwitterion that are embedded in the electric double layer. In turn, we analyze the ion concentration profiles to better understand the relationship between electrolyte structuring within the electric double layer and the structure and energetics of adsorbed cysteine.

Figure 6 shows the concentration, represented as the number density ρ_{solv} , of Na⁺ (in blue) and Cl⁻ ions (in orange) in the aqueous implicit solvent near the electrode surface. The density is calculated as an integral over the xy plane for a given zcoordinate normal to the Au(111) surface. Continuum electric double layer theories would suggest that Na⁺ should accumulate at the electrode surface at negative potentials (i.e., negative electrode surface charge) and that Cl⁻ ions should accumulate near the electrode at positive potentials (i.e, positive electrode surface charge). 88-90 Some of the concentration profiles in Figure 6 are in line with these expectations from continuum theory; however, additional complexities in the concentration profiles arise due to the presence of the cysteine adsorbate on the electrode surface. Beyond a continuum model of the electrolyte, the RISM approach employed herein also accounts for interactions between the solute (i.e., Au(111) and the adsorbed cysteine) and the implicit electrolyte through force-field parameters. Thus, the variance in near-surface ion concentration profiles for different cysteine adsorption configurations suggest that molecular interactions with cysteine significantly impact double layer structuring. Figure 6 also shows that the charged COO⁻ and NH₃ moieties of cysteine zwitterions impact the distribution of electrolyte species near the Au(111) surface.

The cysteine zwitterion affects double layer structuring because the charged COO⁻ and NH₃⁺ functional groups attract the oppositely charged ion in the electrolyte. As a reference, the optimized geometries of each configuration are overlaid on the concentration profiles in Figure 6. Compared to the clean Au(111) surface (Figure 6D,H), the concentration of the counterions is lower in the presence of cysteine, which covers part of the surface. Although we focus on adsorbed cysteine at low coverages in the present work, we note that high-coverage adsorption motifs have been reported. This suggests that at high coverages of adsorbed cysteine, the effects of ions may attenuate as cysteine—cysteine interactions become more dominant. ⁹¹

At a given potential, the concentration of sodium ions for the zw-br(58°) configuration is higher than for the n-br(54°) configuration near the Au surface at $z \sim 6$ Å. For example, Figure 6A,C shows that at -0.45 V vs PZC the near-surface Na⁺ concentrations peak at 0.28 and 0.19 Å⁻¹ for the zw-br(58°) and n-br(54°) configurations, respectively. We observe two peaks in Na⁺ concentration for the zw-br(55°)' configuration at -0.45 V (Figure 6B), in contrast to the two other configurations shown. Of the two Na⁺ peaks for zw-br(55°)', the peak farther away

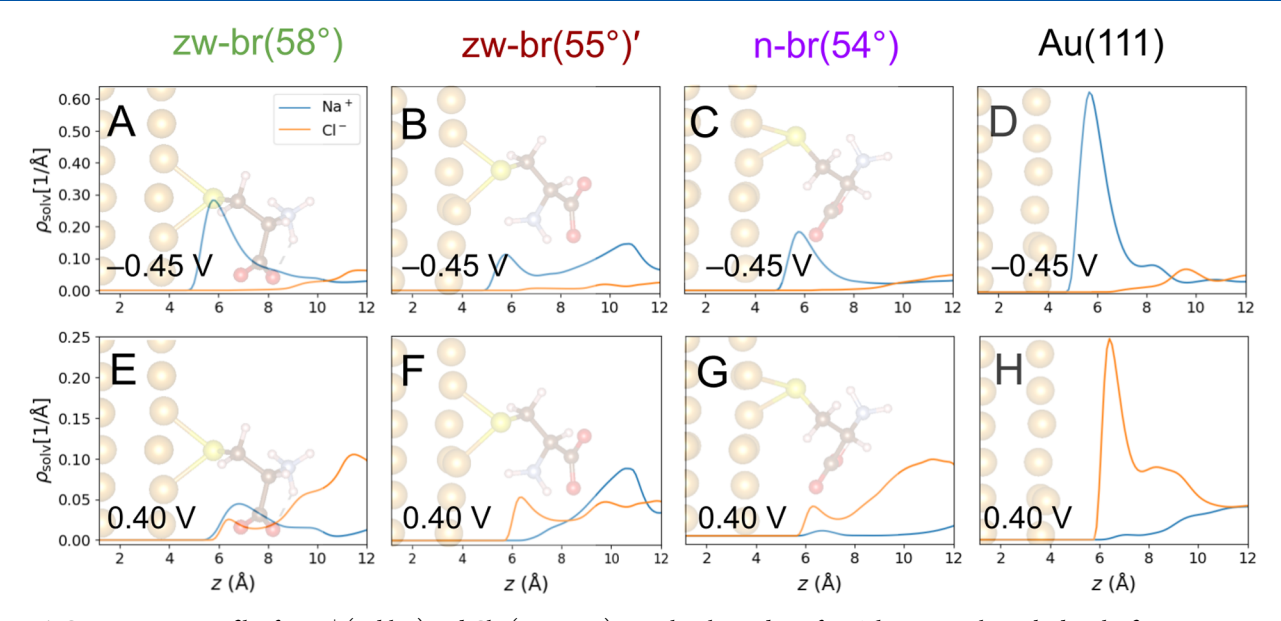


Figure 6. Concentration profiles for Na⁺ (in blue) and Cl⁻ (in orange) near the electrode surface. The potentials marked in the figures are measured relative to PZC. (A, E) zw-br(58°) structure (A) at -0.45 V and (E) at 0.40 V. (B, F) zw-br(55°)′ (B) at -0.45 V and (F) at 0.40 V. (C, G) n-br(54°) (C) at -0.45 V and (G) at 0.40 V. (D, H) Clean Au(111) surface (D) at -0.45 V and (H) at 0.40 V. ρ_{solv} is obtained by integrating the number density of the respective ion over the cross sectional area. Note that all potentials shown are with respect to PZC, as in Figures 3 and 4.

from the surface at \sim 10.7 Å is slightly larger than the peak closer to the surface at \sim 6 Å. Notably, the larger Na⁺ peak at \sim 10.7 Å is positioned <2 Å away from the negatively charged COO-, suggesting favorable Coulombic interactions may be increasing the local Na⁺ concentration near this functional group. At more positive potentials of 0.40 V, however, Figure 6E shows that the near-surface Na⁺ concentration for zw-br(55°)' is significantly attenuated, presumably due to Coulombic repulsion from both the positively charged Au surface and NH₃ functional group. Figure 6G shows that the near-surface Na⁺ concentration is similarly low for the n-br(54°). Figure 6E shows that for the zwbr(58°) configuration at 0.40 V, the Na⁺ concentration is actually a maximum near the Au surface, despite the positive charge on the Au(111) surface. Regarding the Cl⁻ concentration profile at positive potentials of 0.40 V, we observe a large, broad peak around $z \sim 12$ Å for the zw-br(58°) and n-br(54°) configurations (Figure 6E,G). This peak is likely due to the presence of the positively charged NH₃ functional group at these distances. In contrast, the analogous peak is attenuated for zwbr(55°)' because of the negatively charged COO⁻ functional group. Overall, the results in Figure 6 show that the electrode surface charge as well as the charge heterogeneity of cysteine impacts the near-surface electrolyte concentration due to Coulombic attraction and repulsion. The results also imply that other charged biomolecular adsorbates could be used to tune the interfacial electrolyte concentration for tailored electrocatalytic microenvironments. 92-95

To further explore the effects of Coulombic interactions between electrolyte ions and the charged functional groups of cysteine, the Na⁺ ion density is plotted in Figure 7. The density profiles are plotted in the *xy* plane bisecting the carboxylate or carboxylic acid functional group of the different adsorbed cysteine configurations. Figure 7 shows that the Na⁺ ion density is highest near the negatively charged oxygen atoms of the carboxylate and carboxylic acid functional groups of each configuration, which is consistent with the ion concentration profiles shown in Figure 6. Figure 7A,B suggests that the Na⁺ ions are localized between the negatively charged oxygen atoms

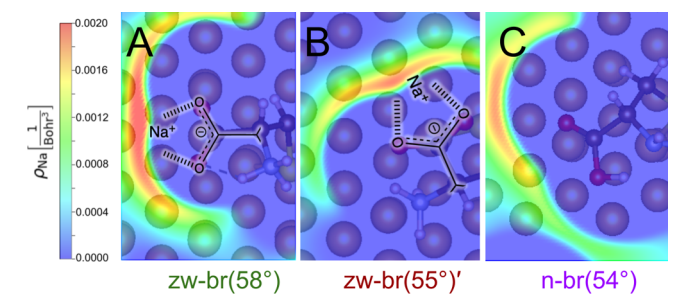


Figure 7. Density of Na⁺ ions at -0.45 V vs PZC near the (A) carboxylate group of zw-br(58°) and (B) the carboxylate group of zw-br(55°)' and (C) the carboxylic acid group of n-br(54°). In this panel, the Na⁺ density is calculated in the *xy* plane parallel to the Au(111) surface at a *z*-coordinate that bisects the carboxylate or carboxylic acid functional group.

of the COO functional group. This finding is consistent with previous experimental and theoretical studies that have shown that sodiated amino acid zwitterions can be stabilized by Na+ ions via a salt bridge configuration in the gas phase. 96 The salt bridge configuration is characterized by a cation bridging the two oxygen atoms of the carboxylate group. In this salt bridge configuration, depicted by the overlaid chemical structures in Figure 7A,B, the carboxylate is stabilized through favorable Coulombic attractions with Na⁺. Figure 7C also shows that the Na^+ density is highest near the carbonyl group of the n-br(54°) configuration. The Na⁺ density profile around the n-br(54°) structure does not resemble the salt bridge structure because the Na+ density maximum is localized near a single oxygen atom, rather than bridging two oxygen atoms. These data suggest that protonation of this functional group weakens its interactions with nearby cations. The favorable salt bridge interactions between Na⁺ helps explain why the zwitterionic zw-br(58°) and zw-br(55°)' structures are in general more stable than the neutral n-br(54°) configuration, especially at more negative potentials when Na⁺ ions are attracted toward the electrode surface.

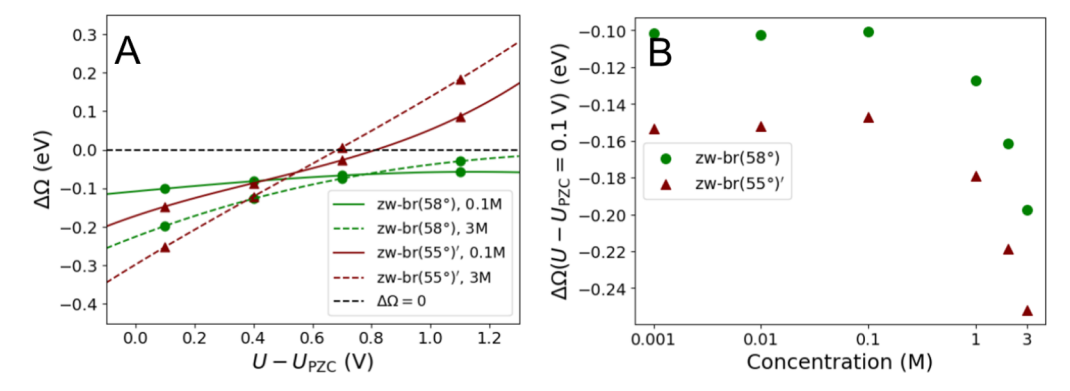


Figure 8. Difference in grand potentials between zwitterionic and neutral cysteine ($\Delta\Omega = \Omega_{zw} - \Omega_n$) as a function of applied potential and electrolyte ionic strength. (A) Difference in grand potentials for 0.1 M NaCl (solid lines) and 3 M NaCl (dashed lines) solutions. The solid lines are a cubic polynomial fit to the computed $\Delta\Omega$ values. The dashed black line is shown to identify $\Delta\Omega = 0$, where the free energies of the zwitterion and neutral configurations are equivalent. (B) Difference in grand potential at 0.1 V vs PZC with varying NaCl concentrations.

At positive potentials, chloride ions are attracted to the positively charged surface (Figure 6D-F); however, these chloride anions also destabilize the COO⁻ functional group of zwitterion structures. As shown in Figure S7A for the zwbr(58°) at 0.40 V, the Cl⁻ density is highest near NH₃ and is repelled by the anionic COO⁻ moiety. For this system, there are also peaks in the Cl density associated with ion-pairing interactions with near-surface Na⁺ ions. There is a high Na⁺ concentration near the surface for the zw-br(58°) structure at 0.40 V (Figure 6D) due to salt bridge interactions between COO- and Na+. Figure S7B shows that the Cl- density is depleted near n-br(54°). For zwitterionic cysteine systems at positive potentials, Na+ ions also accumulate near the surface to stabilize the COO⁻ group via the aforementioned salt bridge structure. Meanwhile, there is also Coloumbic repulsion between the Na⁺ cations and the positively charged surface. In turn, the zw-br(58°) and n-br(54°) configurations are nearly degenerate at positive potentials. At potentials positive of ~ 0.50 V, however, the zw-br $(55^{\circ})'$ is higher in free energy than the nbr(54°) because of repulsive interactions between the NH₃+ group with the surface.

Because electrolyte ions appear to preferentially stabilize zwitterionic cysteine over neutral cysteine, we analyzed further the effects of electrolyte concentration on stability trends. To quantify these effects, we calculated the difference in grand potentials between the two most stable zwitterion structures and the neutral n-br(54°) configuration as a function of applied potential U.

$$\Delta\Omega(U) = \Omega_{zw}(U) - \Omega_{n}(U) \tag{3}$$

where $\Omega_{\rm zw}$ is the grand potential of a given cysteine zwitterion structure and $\Omega_{\rm n}$ is the grand potential of the n-br(54°) configuration. As defined in eq 3, a negative value of $\Delta\Omega$ indicates that the specified zwitterion is more thermodynamically stable than the neutral n-br(54°) configuration at a given potential U.

Figure 8 shows the effect of electrolyte ionic strength on the calculated free energy difference between the zwitterionic structures and neutral cysteine, $\Delta\Omega$. The results in Figure 8 show that the electrolyte concentration impacts the relative stability of neutral and zwitterionic cysteine. For example, Figure 8B shows that at 0.1 V vs PZC, the calculated $\Delta\Omega$ for both zwbr(58°) and zw-br(55°)′ becomes more negative with increasing bulk NaCl concentration. This is because the increased bulk NaCl concentration also increases the Na⁺ ion

concentration near the surface (Figure S6), further stabilizing the zwitterion. Notably, this trend in $\Delta\Omega$ with NaCl concentration is inverted at positive potentials. Figure 8A shows that at more positive potentials, the $\Delta\Omega$ is more negative for the 0.1 M solution than for the 3 M solution. The data show that the anion concentration near the surface increases with higher potentials, which could in principle stabilize the zwitterion through Coulombic attraction to the cationic NH₃⁺ funcitonal group. Yet, the zwitterion is actually destabilized by higher ion concentrations at these high potentials. Specifically, at potentials positive of 0.82 and 0.70 V, the n-br(54°) configuration is lower in free energy than the zw-br(55°)' configuration at 0.1 and 3 M, respectively. This implies that among the ion pairing interactions between the cysteine zwitterion and the electrolyte ions, the salt-bridge interactions between COO and Na are stronger than the NH₃/Cl interactions. In general, Figure 8B shows that the calculated $\Delta\Omega$ values have greater potential dependence for higher NaCl concentrations. These observations highlight the impact that ionic strength can have on the potential-dependent thermodynamics of adsorbates on electrode surfaces.

While the calculated $\Delta\Omega$ between the zwitterionic and neutral adsorption structures is due in part to the ions in the electrolyte, there remains a free energy difference even for very dilute electrolytes, as shown in Figure 8B. Figure 8B shows that while the $\Delta\Omega$ decreases considerably for concentrations greater than 1 M, the $\Delta\Omega$ converges to approximately constant values below concentrations of ~0.1 M NaCl. Example concentration profiles along the entire length of the expanded unit cells are shown in Figure S9. At very low NaCl concentrations, the $\Delta\Omega$ converges to ~0.10 and ~0.14 eV for the zw-br(58°) and zw-br(55°)′ configurations, respectively. Thus, the free energy difference between the neutral and zwitterionic cysteine adsorbates cannot solely be attributed to ion effects.

We attribute the plateau in $\Delta\Omega$ at low ionic strength to differences in the solvation energies and the Coulombic interactions with the Au surface. Energetic differences persist in the absence of electrolyte ions in part because zwitterionic amino acids have larger solvation energies in water than their neutral analogues. Theoretical calculations have shown that four water molecules around proline makes its zwitterion \sim 0.11 eV more stable than its neutral form while a fifth water molecule makes the zwitterion 0.26 eV more stable. The $\Delta\Omega$ of \sim 0.10 eV at low ionic strength is at the lower bound of the solvation energy differences calculated for proline using explicit water

molecules. We note that when adsorbed to the Au surface, fewer water molecules can solvate cysteine due to the two-dimensional structure of the electrode-electrolyte interface. The charged functional groups of the zwitterion also exhibit either Coulombic attractions or repulsions with the electrode surface. Because these data are shown at 0.10 V, which is \sim 0.1 V positive of the PZC of zw-br(58°), the near-surface COO incurs additional stabilization due to Coulombic attraction to the modest positive charge on the Au surface. We observe similar trends using CsCl and NaOH in the implicit RISM electrolyte (Figure S5). As discussed in Section S3 of the Supporting Information, we do not observe significantly different thermodynamic trends between NaCl, NaOH and CsCl electrolytes; however, there are some differences in the double layer concentration profiles of these systems. Notably, the nearsurface cation concentration is attenuated for the CsCl system. Interfacial cations are likely dehydrated due to more favorable interactions with cysteine (Figure 7) and in turn, the reduced near-surface Cs⁺ concentration may be attributed to cation size effects. Further details are provided in Section S3 of the Supporting Information. Together, these results suggest that the structure of adsorbed cysteine and the associated energetics are strongly linked to interfacial electrostatics and electrolyte structuring within the electrical double layer. The RISM solvation model used herein reveals information about the distribution and orientation of the solvent and electrolyte and provides a computationally efficient means to predicting electric double layer structure in computational interfacial electrochemistry. Additional insights into adsorbate-electrolyte interactions could be obtained in future studies through the inclusion of explicit water molecules or by electrostatic embedding in classical molecular dynamics simulations. 48,51,5

CONCLUSIONS

In this work, we analyzed the effect of applied potential and electrolyte concentration on the structure and stability of adsorbed cysteine on Au(111). We used the ESM-RISM method to perform constant-potential periodic DFT calculations with a classical representation of the electrolyte solvent and ions. This theoretical approach enabled a description of potential-dependent interfacial thermodynamics and ion structuring. The applied potential influences the structure of adsorbed cysteine at electrochemical interfaces via the adsorbate's Coulombic interactions between the charged electrode surface and the ions in the electrolyte. Zwitterionic cysteine is lower in free energy than neutral cysteine over the range of potentials studied, although the relative population of neutral cysteine is calculated to increase for more positive applied potentials. The COO⁻ functional group of the cysteine zwitterion is oriented toward the surface at positive potentials, whereas the NH₃ functional group is oriented toward the surface at negative potentials. At more negative potentials, the zwitterion is further stabilized with higher electrolyte ionic strength due to electrostatically favorable salt-bridge ion pairing interactions between the COO functional group and Na⁺ ions. This trend is reversed at more positive potentials, where the zwitterionic configurations are destabilized with increasing ionic strength because of the weaker attractions between the NH₃ functional group and the near-surface Cl ions. This study demonstrates how the applied potential can be used to modify the structure of adsorbed amino acids on solid surfaces. Furthermore, the results herein suggest that adsorbed amino acids, peptides, or other biomolecules can be used to tune

electrolyte composition at the electrochemical interface, which could be an approach to design tailored microenvironments for electrochemical separations and catalysis. ^{93–95} Because cysteine can adsorb to metal surfaces through its thiol headgroup, it can be used as a linker for specific polypeptide functionalized electrochemical interfaces. Employing acidic or basic amino acid residues within adsorbed polypeptides could be one approach to control the molecular structure of the electric double layer. This work demonstrates the critical role of the applied potential and interfacial electrolyte structure on the structure of biomolecular adsorbates on solid surfaces.

ASSOCIATED CONTENT

Supporting Information

The Supporting Information is available free of charge at https://pubs.acs.org/doi/10.1021/acs.jpcc.4c04216.

Cysteine adsorption in vacuum, grand potential calculations of additional adsorbed cysteine configurations, effects of different electrolyte ions, interfacial dipole moment and potential of zero free charge, and sample Quantum ESPRESSO input file (PDF)

CIF files for converged cysteine adsorption configurations (ZIP)

AUTHOR INFORMATION

Corresponding Author

Robert E. Warburton – Department of Chemical and Biomolecular Engineering, Case Western Reserve University, Cleveland, Ohio 44106, United States; orcid.org/0000-0002-9693-307X; Email: rew134@case.edu

Authors

Hari R. Sudhakar — Department of Chemical and Biomolecular Engineering, Case Western Reserve University, Cleveland, Ohio 44106, United States; Department of Chemical Engineering, Indian Institute of Technology Bombay, Mumbai, Maharashtra 400076, India

Julie N. Renner — Department of Chemical and Biomolecular Engineering, Case Western Reserve University, Cleveland, Ohio 44106, United States; orcid.org/0000-0002-6140-4346

Complete contact information is available at: https://pubs.acs.org/10.1021/acs.jpcc.4c04216

Notes

The authors declare no competing financial interest.

ACKNOWLEDGMENTS

This work was supported by start-up funding from the Case School of Engineering at Case Western Reserve University. This work made use of the High Performance Computing Resource in the Core Facility for Advanced Research Computing at Case Western Reserve University. J.N.R. acknowledges support from the National Science Foundation Awards 2045033 and 2026259. We acknowledge Brandon Bukowski, Zeynep Bagbudar, Mahmudul Hasan, and Noah South for helpful discussions.

REFERENCES

- (1) Kasemo, B. Biological surface science. Surf. Sci. 2002, 500, 656–677.
- (2) Ogawa, K.; Tsujibayashi, T.; Takahashi, K.; Azuma, J.; Ichimiya, M.; Fujimoto, H.; Sumimoto, M.; Kamada, M. Photoelectron

- spectroscopic study on the electronic structures of the dental gold alloys and their interaction with L-cysteine. *J. Appl. Phys.* **2011**, *110*, 103718.
- (3) Eralp, T.; Shavorskiy, A.; Held, G. The adsorption geometry and chemical state of lysine on Cu{110}. Surf. Sci. 2011, 605, 468–472.
- (4) Eralp, T.; Shavorskiy, A.; Zheleva, Z. V.; Held, G.; Kalashnyk, N.; Ning, Y.; Linderoth, T. R. Global and Local Expression of Chirality in Serine on the Cu{110} Surface. *Langmuir* **2010**, *26*, 18841–18851.
- (5) Eralp, T.; Shavorskiy, A.; Zheleva, Z. V.; Dhanak, V. R.; Held, G. Hydrogen Bond-Induced Pair Formation of Glycine on the Chiral Cu{531} Surface. *Langmuir* **2010**, *26*, 10918–10923.
- (6) Chen, Q.; Frankel, D. J.; Richardson, N. V. Self-Assembly of Adenine on Cu(110) Surfaces. *Langmuir* **2002**, *18*, 3219–3225.
- (7) Ismail, K. M. Evaluation of cysteine as environmentally friendly corrosion inhibitor for copper in neutral and acidic chloride solutions. *Electrochim. Acta* **2007**, *52*, 7811–7819.
- (8) Ritchie, S. M. C.; Kissick, K. E.; Bachas, L. G.; Sikdar, S. K.; Parikh, C.; Bhattacharyya, D. Polycysteine and Other Polyamino Acid Functionalized Microfiltration Membranes for Heavy Metal Capture. *Environ. Sci. Technol.* **2001**, *35*, 3252–3258.
- (9) Liu, A.-C.; Chen, D.-C.; Lin, C.-C.; Chou, H.-H.; Chen, C.-H. Application of Cysteine Monolayers for Electrochemical Determination of Sub-ppb Copper(II). *Anal. Chem.* **1999**, *71*, 1549–1552.
- (10) Loney, C. N.; Maheshwari, S.; Pramounmat, N.; Janik, M. J.; Renner, J. N. Effects of Peptide-Functionalized Surfaces on the Electrochemical Hydrogen Evolution Reaction. *J. Electrochem. En. Conv. Stor.* **2020**, *17*, No. 040801.
- (11) Biriukov, D.; Futera, Z. Adsorption of Amino Acids at the Gold/Aqueous Interface: Effect of an External Electric Field. *J. Phys. Chem. C* **2021**, *125*, 7856–7867.
- (12) Whelan, C. M.; Barnes, C. J.; Grégoire, C.; Pireaux, J. J. The influence of step sites on the bonding of benzenethiol on Au surfaces. *Surf. Sci.* **2000**, *454*–*456*, *67*–*72*.
- (13) Nuzzo, R. G.; Dubois, L. H.; Allara, D. L. Fundamental studies of microscopic wetting on organic surfaces. 1. Formation and structural characterization of a self-consistent series of polyfunctional organic monolayers. *J. Am. Chem. Soc.* **1990**, *112*, 558–569.
- (14) Kondoh, H.; Kodama, C.; Nozoye, H. Structure-Dependent Change of Desorption Species from n-Alkanethiol Monolayers Adsorbed on Au(111): Desorption of Thiolate Radicals from Low-Density Structures. *J. Phys. Chem. B* **1998**, *102*, 2310–2312.
- (15) Grönbeck, H.; Curioni, A.; Andreoni, W. Thiols and Disulfides on the Au(111) Surface: The Headgroup-Gold Interaction. *J. Am. Chem. Soc.* **2000**, *122*, 3839–3842.
- (16) Vallee, A.; Humblot, V.; Pradier, C.-M. Peptide Interactions with Metal and Oxide Surfaces. *Acc. Chem. Res.* **2010**, *43*, 1297–1306.
- (17) Chi, Q.; Zhang, J.; Nielsen, J. U.; Friis, E. P.; Chorkendorff, I.; Canters, G. W.; Andersen, J. E. T.; Ulstrup, J. Molecular Monolayers and Interfacial Electron Transfer of Pseudomonas aeruginosa Azurin on Au(111). J. Am. Chem. Soc. 2000, 122, 4047–4055.
- (18) Berg, J. M.; Tymoczko, J. L.; Stryer, L. *Biochemistry*; Macmillan,
- (19) Brolo, A. G.; Germain, P.; Hager, G. Investigation of the Adsorption of l-Cysteine on a Polycrystalline Silver Electrode by Surface-Enhanced Raman Scattering (SERS) and Surface-Enhanced Second Harmonic Generation (SESHG). J. Phys. Chem. B 2002, 106, 5982–5987.
- (20) LeParc, R.; Smith, C. I.; Cuquerella, M. C.; Williams, R. L.; Fernig, D. G.; Edwards, C.; Martin, D. S.; Weightman, P. Reflection Anisotropy Spectroscopy Study of the Adsorption of Sulfur-Containing Amino Acids at the Au(110)/Electrolyte Interface. *Langmuir* **2006**, 22, 3413–3420.
- (21) Di Felice, R.; Selloni, A.; Molinari, E. DFT Study of Cysteine Adsorption on Au(111). J. Phys. Chem. B 2003, 107, 1151–1156.
- (22) Di Felice, R.; Selloni, A. Adsorption modes of cysteine on Au(111): Thiolate, amino-thiolate, disulfide. *J. Chem. Phys.* **2004**, *120*, 4906–4914
- (23) Uvdal, K.; Bodö, P.; Liedberg, B. l-cysteine adsorbed on gold and copper: An X-ray photoelectron spectroscopy study. *J. Colloid Interface Sci.* **1992**, *149*, 162–173.

- (24) Isted, G. E.; Martin, D. S.; Smith, C. I.; LeParc, R.; Cole, R. J.; Weightman, P. The adsorption of L-cysteine on Au(110) in ultra-high vacuum and electrochemical environments. *Phys. Status Solidi C* **2005**, 2, 4012–4016.
- (25) Höffling, B.; Ortmann, F.; Hannewald, K.; Bechstedt, F. Single cysteine adsorption on Au(110): A first-principles study. *Phys. Rev. B* **2010**, *81*, No. 045407.
- (26) Ihs, A.; Liedberg, B. Chemisorption of l-cysteine and 3-mercaptopropionic acid on gold and copper surfaces: An infrared reflection-absorption study. *J. Colloid Interface Sci.* **1991**, *144*, 282–292.
- (27) Jürgensen, A.; Raschke, H.; Esser, N.; Hergenröder, R. An in situ XPS study of L-cysteine co-adsorbed with water on polycrystalline copper and gold. *Appl. Surf. Sci.* **2018**, 435, 870–879.
- (28) Che, F.; Gray, J. T.; Ha, S.; Kruse, N.; Scott, S. L.; McEwen, J.-S. Elucidating the Roles of Electric Fields in Catalysis: A Perspective. *ACS Catal.* **2018**, *8*, 5153–5174.
- (29) Ryu, J.; Surendranath, Y. Tracking Electrical Fields at the Pt/H2O Interface during Hydrogen Catalysis. *J. Am. Chem. Soc.* **2019**, *141*, 15524–15531.
- (30) Shetty, M.; Ardagh, M. A.; Pang, Y.; Abdelrahman, O. A.; Dauenhauer, P. J. Electric-Field-Assisted Modulation of Surface Thermochemistry. *ACS Catal.* **2020**, *10*, 12867–12880.
- (31) Warburton, R. E.; Hutchison, P.; Jackson, M. N.; Pegis, M. L.; Surendranath, Y.; Hammes-Schiffer, S. Interfacial Field-Driven Proton-Coupled Electron Transfer at Graphite-Conjugated Organic Acids. *J. Am. Chem. Soc.* **2020**, *142*, 20855–20864.
- (32) Wan, M.; Yue, H.; Notarangelo, J.; Liu, H.; Che, F. Deep Learning-Assisted Investigation of Electric Field—Dipole Effects on Catalytic Ammonia Synthesis. *JACS Au* **2022**, *2*, 1338—1349.
- (33) Menachekanian, S.; Voegtle, M. J.; Warburton, R. E.; Hammes-Schiffer, S.; Dawlaty, J. M. Inductive Effect Alone Cannot Explain Lewis Adduct Formation and Dissociation at Electrode Interfaces. *J. Am. Chem. Soc.* **2023**, *145*, 5759–5768.
- (34) Westendorff, K. S.; Hülsey, M. J.; Wesley, T. S.; Román-Leshkov, Y.; Surendranath, Y. Electrically driven proton transfer promotes Brønsted acid catalysis by orders of magnitude. *Science* **2024**, *383*, 757–763.
- (35) Hager, G.; Brolo, A. G. Protonation and deprotonation of cysteine and cystine monolayers probed by impedance spectroscopy. *J. Electroanal. Chem.* **2009**, *625*, 109–116.
- (36) Otani, M.; Sugino, O. First-principles calculations of charged surfaces and interfaces: A plane-wave nonrepeated slab approach. *Phys. Rev. B* **2006**, *73*, No. 115407.
- (37) Nishihara, S.; Otani, M. Hybrid solvation models for bulk, interface, and membrane: Reference interaction site methods coupled with density functional theory. *Phys. Rev. B* **2017**, *96*, No. 115429.
- (38) Giannozzi, P.; Baroni, S.; Bonini, N.; Calandra, M.; Car, R.; Cavazzoni, C.; Ceresoli, D.; Chiarotti, G. L.; Cococcioni, M.; Dabo, I.; et al. QUANTUM ESPRESSO: a modular and open-source software project for quantum simulations of materials. *J. Phys.: Condens. Matter* **2009**, *21*, No. 395502.
- (39) Giannozzi, P.; Andreussi, O.; Brumme, T.; Bunau, O.; Buongiorno Nardelli, M.; Calandra, M.; Car, R.; Cavazzoni, C.; Ceresoli, D.; Cococcioni, M.; Colonna, N.; Carnimeo, I.; Dal Corso, A.; de Gironcoli, S.; Delugas, P.; DiStasio, R. A.; Ferretti, A.; Floris, A.; Fratesi, G.; Fugallo, G.; Gebauer, R.; Gerstmann, U.; Giustino, F.; Gorni, T.; Jia, J.; Kawamura, M.; Ko, H. Y.; Kokalj, A.; Küçükbenli, E.; Lazzeri, M.; Marsili, M.; Marzari, N.; Mauri, F.; Nguyen, N. L.; Nguyen, H. V.; Otero-de-la-Roza, A.; Paulatto, L.; Poncé, S.; Rocca, D.; Sabatini, R.; Santra, B.; Schlipf, M.; Seitsonen, A. P.; Smogunov, A.; Timrov, I.; Thonhauser, T.; Umari, P.; Vast, N.; Wu, X.; Baroni, S.; et al. Advanced capabilities for materials modelling with Quantum ESPRESSO. *J. Phys.: Condens. Matter* 2017, 29, 465901.
- (40) Perdew, J. P.; Burke, K.; Ernzerhof, M. Generalized Gradient Approximation Made Simple. *Phys. Rev. Lett.* **1996**, *77*, 3865–3868.
- (41) Grimme, S.; Antony, J.; Ehrlich, S.; Krieg, H. A consistent and accurate ab initio parametrization of density functional dispersion correction (DFT-D) for the 94 elements H-Pu. *J. Chem. Phys.* **2010**, 132, 154104.

- (42) Blöchl, P. E. Projector augmented-wave method. *Phys. Rev. B* **1994**, *50*, 17953–17979.
- (43) Dal Corso, A. Pseudopotentials periodic table: From H to Pu. Comput. Mater. Sci. 2014, 95, 337–350.
- (44) Hagiwara, S.; Nishihara, S.; Kuroda, F.; Otani, M. Development of a dielectrically consistent reference interaction site model combined with the density functional theory for electrochemical interface simulations. *Phys. Rev. Mater.* **2022**, *6*, No. 093802.
- (45) Maldonado, A. M.; Hagiwara, S.; Choi, T. H.; Eckert, F.; Schwarz, K.; Sundararaman, R.; Otani, M.; Keith, J. A. Quantifying Uncertainties in Solvation Procedures for Modeling Aqueous Phase Reaction Mechanisms. *J. Phys. Chem. A* **2021**, *125*, 154–164.
- (46) Tesch, R.; Kowalski, P. M.; Eikerling, M. H. Properties of the Pt(111)/electrolyte electrochemical interface studied with a hybrid DFT-solvation approach. *J. Phys.: Condens. Matter* **2021**, *33*, 444004.
- (47) Ringe, S.; Hörmann, N. G.; Oberhofer, H.; Reuter, K. Implicit Solvation Methods for Catalysis at Electrified Interfaces. *Chem. Rev.* **2022**, *122*, 10777–10820.
- (48) Abidi, N.; Steinmann, S. N. An Electrostatically Embedded QM/MM Scheme for Electrified Interfaces. *ACS Appl. Mater. Interfaces* **2023**, *15*, 25009–25017.
- (49) Groß, A.; Sakong, S. Ab Initio Simulations of Water/Metal Interfaces. *Chem. Rev.* **2022**, *122*, 10746–10776.
- (50) Haruyama, J.; Ikeshoji, T.; Otani, M. Electrode potential from density functional theory calculations combined with implicit solvation theory. *Phys. Rev. Mater.* **2018**, *2*, No. 095801.
- (51) Sugino, O.; Hamada, I.; Otani, M.; Morikawa, Y.; Ikeshoji, T.; Okamoto, Y. First-principles molecular dynamics simulation of biased electrode/solution interface. *Surf. Sci.* **2007**, *601*, 5237–5240.
- (52) Otani, M.; Hamada, I.; Sugino, O.; Morikawa, Y.; Okamoto, Y.; Ikeshoji, T. Structure of the water/platinum interface—-a first principles simulation under bias potential. *Phys. Chem. Chem. Phys.* **2008**, *10*, 3609–3612.
- (53) Kovalenko, A.; Hirata, F. Potentials of mean force of simple ions in ambient aqueous solution. I. Three-dimensional reference interaction site model approach. *J. Chem. Phys.* **2000**, *112*, 10391–10402.
- (54) Dang, L. X. The nonadditive intermolecular potential for water revised. *J. Chem. Phys.* **1992**, *97*, 2659–2660.
- (55) Smith, D. E.; Dang, L. X. Computer simulations of NaCl association in polarizable water. *J. Chem. Phys.* **1994**, *100*, 3757–3766.
- (56) Matsugami, M.; Yoshida, N.; Hirata, F. Theoretical characterization of the "ridge" in the supercritical region in the fluid phase diagram of water. *J. Chem. Phys.* **2014**, *140*, 104511.
- (57) Rappe, A. K.; Casewit, C. J.; Colwell, K. S.; Goddard, W. A. I.; Skiff, W. M. UFF, a full periodic table force field for molecular mechanics and molecular dynamics simulations. *J. Am. Chem. Soc.* **1992**, *114*, 10024–10035.
- (58) Bonnet, N.; Morishita, T.; Sugino, O.; Otani, M. First-Principles Molecular Dynamics at a Constant Electrode Potential. *Phys. Rev. Lett.* **2012**, *109*, No. 266101.
- (59) Chattopadhyay, A.; Boxer, S. G. Vibrational Stark Effect Spectroscopy. *J. Am. Chem. Soc.* **1995**, 117, 1449–1450.
- (60) Fried, S. D.; Boxer, S. G. Measuring Electric Fields and Noncovalent Interactions Using the Vibrational Stark Effect. *Acc. Chem. Res.* **2015**, *48*, 998–1006.
- (61) Sorenson, S. A.; Patrow, J. G.; Dawlaty, J. M. Solvation Reaction Field at the Interface Measured by Vibrational Sum Frequency Generation Spectroscopy. *J. Am. Chem. Soc.* **2017**, *139*, 2369–2378.
- (62) Goldsmith, Z. K.; Secor, M.; Hammes-Schiffer, S. Inhomogeneity of Interfacial Electric Fields at Vibrational Probes on Electrode Surfaces. *ACS Cent. Sci.* **2020**, *6*, 304–311.
- (63) Sarkar, S.; Maitra, A.; Lake, W. R.; Warburton, R. E.; Hammes-Schiffer, S.; Dawlaty, J. M. Mechanistic Insights about Electrochemical Proton-Coupled Electron Transfer Derived from a Vibrational Probe. *J. Am. Chem. Soc.* **2021**, *143*, 8381–8390.
- (64) Lake, W. R.; Meng, J.; Dawlaty, J. M.; Lian, T.; Hammes-Schiffer, S. Electro-inductive Effect Dominates Vibrational Frequency Shifts of

- Conjugated Probes on Gold Electrodes. J. Am. Chem. Soc. 2023, 145, 22548-22554.
- (65) Fafarman, A. T.; Sigala, P. A.; Schwans, J. P.; Fenn, T. D.; Herschlag, D.; Boxer, S. G. Quantitative, directional measurement of electric field heterogeneity in the active site of ketosteroid isomerase. *Proc. Natl. Acad. Sci. U. S. A.* **2012**, *109*, E299–E308.
- (66) Dodero, G.; De Michieli, L.; Cavalleri, O.; Rolandi, R.; Oliveri, L.; Daccà, A.; Parodi, R. l-Cysteine chemisorption on gold: an XPS and STM study. *Colloids Surf. A: Physicochem. Eng. Asp.* **2000**, *175*, 121–128
- (67) Cavalleri, O.; Gonella, G.; Terreni, S.; Vignolo, M.; Pelori, P.; Floreano, L.; Morgante, A.; Canepa, M.; Rolandi, R. High resolution XPS of the S 2p core level region of the L-cysteine/gold interface. *J. Phys.: Condens. Matter* **2004**, *16*, S2477.
- (68) Hjorth Larsen, A.; Jørgen Mortensen, J.; Blomqvist, J.; Castelli, I. E.; Christensen, R.; Dułak, M.; Friis, J.; Groves, M. N.; Hammer, B.; Hargus, C.; Hermes, E. D.; Jennings, P. C.; Bjerre Jensen, P.; Kermode, J.; Kitchin, J. R.; Leonhard Kolsbjerg, E.; Kubal, J.; Kaasbjerg, K.; Lysgaard, S.; Bergmann Maronsson, J.; Maxson, T.; Olsen, T.; Pastewka, L.; Peterson, A.; Rostgaard, C.; Schiøtz, J.; Schütt, O.; Strange, M.; Thygesen, K. S.; Vegge, T.; Vilhelmsen, L.; Walter, M.; Zeng, Z.; Jacobsen, K. W.; et al. The atomic simulation environment—a Python library for working with atoms. *J. Phys.: Condens. Matter* 2017, 29, 273002.
- (69) Martí, C.; Blanck, S.; Staub, R.; Loehlé, S.; Michel, C.; Steinmann, S. N. DockOnSurf: A Python Code for the High-Throughput Screening of Flexible Molecules Adsorbed on Surfaces. *J. Chem. Inf. Model.* **2021**, *61*, 3386–3396.
- (70) Deshpande, S.; Maxson, T.; Greeley, J. Graph theory approach to determine configurations of multidentate and high coverage adsorbates for heterogeneous catalysis. *npj Comput. Mater.* **2020**, *6*, 79.
- (71) Ramachandran, G. N.; Ramakrishnan, C.; Sasisekharan, V. Stereochemistry of polypeptide chain configurations. *J. Mol. Biol.* **1963**, 7, 95–99.
- (72) Shin, T.; Kim, K.-N.; Lee, C.-W.; Shin, S. K.; Kang, H. Self-Assembled Monolayer of l-Cysteine on Au(111): Hydrogen Exchange between Zwitterionic l-Cysteine and Physisorbed Water. *J. Phys. Chem. B* **2003**, *107*, 11674–11681.
- (73) Gonella, G.; Terreni, S.; Cvetko, D.; Cossaro, A.; Mattera, L.; Cavalleri, O.; Rolandi, R.; Morgante, A.; Floreano, L.; Canepa, M. Ultrahigh Vacuum Deposition of l-Cysteine on Au(110) Studied by High-Resolution X-ray Photoemission: From Early Stages of Adsorption to Molecular Organization. *J. Phys. Chem. B* **2005**, *109*, 18003–18009.
- (74) Kučera, J.; Gross, A. Adsorption of 4-Mercaptopyridine on Au(111): A Periodic DFT Study. *Langmuir* **2008**, 24, 13985–13992.
- (75) Ge, A.; Kastlunger, G.; Meng, J.; Lindgren, P.; Song, J.; Liu, Q.; Zaslavsky, A.; Lian, T.; Peterson, A. A. On the Coupling of Electron Transfer to Proton Transfer at Electrified Interfaces. *J. Am. Chem. Soc.* **2020**, *142*, 11829–11834.
- (76) Pasumarthi, V.; Yu, H.; Akhade, S. A.; Abild-Pedersen, F.; Varley, J. B.; Bajdich, M. A Comparative Study of Electrical Double Layer Effects for $\rm CO_2$ Reduction Reaction Kinetics. *J. Phys. Chem. C* **2023**, 127, 16850–16860.
- (77) Yu, H.; Weitzner, S. E.; Varley, J. B.; Wood, B. C.; Akhade, S. A. Surface Engineering of Copper Catalyst through CO* Adsorbate. *J. Phys. Chem. C* 2023, 127, 1789–1797.
- (78) Weitzner, S. E.; Akhade, S. A.; Varley, J. B.; Wood, B. C.; Otani, M.; Baker, S. E.; Duoss, E. B. Toward Engineering of Solution Microenvironments for the CO₂ Reduction Reaction: Unraveling pH and Voltage Effects from a Combined Density-Functional—Continuum Theory. *J. Phys. Chem. Lett.* **2020**, *11*, 4113—4118.
- (79) Hasegawa, T.; Hagiwara, S.; Otani, M.; Maeda, S. A Combined Reaction Path Search and Hybrid Solvation Method for the Systematic Exploration of Elementary Reactions at the Solid—Liquid Interface. *J. Phys. Chem. Lett.* **2023**, *14*, 8796—8804.
- (80) Haruyama, J.; Ikeshoji, T.; Otani, M. Analysis of Lithium Insertion/Desorption Reaction at Interfaces between Graphite Electro-

- des and Electrolyte Solution Using Density Functional + Implicit Solvation Theory. J. Phys. Chem. C 2018, 122, 9804–9810.
- (81) Schmickler, W.; Santos, E. *Interfacial Electrochemistry*; Springer: Berlin, Heidelberg, 2010.
- (82) Hörmann, N. G.; Andreussi, O.; Marzari, N. Grand canonical simulations of electrochemical interfaces in implicit solvation models. *J. Chem. Phys.* **2019**, *150*, No. 041730.
- (83) Chan, K.; Nørskov, J. K. Electrochemical Barriers Made Simple. *J. Phys. Chem. Lett.* **2015**, *6*, 2663–2668.
- (84) Gauthier, J. A.; Dickens, C. F.; Heenen, H. H.; Vijay, S.; Ringe, S.; Chan, K. Unified Approach to Implicit and Explicit Solvent Simulations of Electrochemical Reaction Energetics. *J. Chem. Theory Comput.* **2019**, *15*, 6895–6906.
- (85) Hutchison, P.; Warburton, R. E.; Soudackov, A. V.; Hammes-Schiffer, S. Multicapacitor Approach to Interfacial Proton-Coupled Electron Transfer Thermodynamics at Constant Potential. *J. Phys. Chem. C* 2021, 125, 21891–21901.
- (86) Agrawal, N.; Wong, A. J.-W.; Maheshwari, S.; Janik, M. J. An efficient approach to compartmentalize double layer effects on kinetics of interfacial proton-electron transfer reactions. *J. Catal.* **2024**, *430*, No. 115360.
- (87) Kaur, J.; Kant, R. Model of Local Work Function and PZC for Molecular Self Assembly over Nanostructured Metal Electrode. *J. Phys. Chem. C* **2018**, *122*, 911–918.
- (88) Bard, A. J.; Faulkner, L. R. *Electrochemical methods and applications*, 2nd ed.; Wiley-Interscience: New York, 2000; OCLC: 45314787.
- (89) Gouy, M. Sur la constitution de la charge électrique à la surface d'un électrolyte. *J. Phys. Theor. Appl.* **1910**, *9*, 457–468.
- (90) Stern, O. The theory of the electrolytic double shift. Z. Elektrochem. Angew. Phys. Chem. 1924, 30, 508-516.
- (91) Mom, R. V.; Melissen, S. T. A. G.; Sautet, P.; Frenken, J. W. M.; Steinmann, S. N.; Groot, I. M. N. The Pressure Gap for Thiols: Methanethiol Self-Assembly on Au(111) from Vacuum to 1 bar. *J. Phys. Chem. C* 2019, 123, 12382–12389.
- (92) Zhang, H.; Gao, J.; Raciti, D.; Hall, A. S. Promoting Cu-catalysed CO_2 electroreduction to multicarbon products by tuning the activity of H_2O . *Nat. Catal.* **2023**, *6*, 807–817.
- (93) Miller, D. M.; Abels, K.; Guo, J.; Williams, K. S.; Liu, M. J.; Tarpeh, W. A. Electrochemical Wastewater Refining: A Vision for Circular Chemical Manufacturing. *J. Am. Chem. Soc.* **2023**, *145*, 19422–19439.
- (94) Kim, C.; Bui, J. C.; Luo, X.; Cooper, J. K.; Kusoglu, A.; Weber, A. Z.; Bell, A. T. Tailored catalyst microenvironments for CO2 electroreduction to multicarbon products on copper using bilayer ionomer coatings. *Nat. Energy* **2021**, *6*, 1026–1034.
- (95) Schreier, M.; Kenis, P.; Che, F.; Hall, A. S. Trends in Electrocatalysis: The Microenvironment Moves to Center Stage. *ACS Energy Lett.* **2023**, *8*, 3935–3940.
- (96) Wyttenbach, T.; Witt, M.; Bowers, M. T. On the Stability of Amino Acid Zwitterions in the Gas Phase: The Influence of Derivatization, Proton Affinity, and Alkali Ion Addition. *J. Am. Chem. Soc.* **2000**, *122*, 3458–3464.
- (97) Bachrach, S. M.; Nguyen, T. T.; Demoin, D. W. Microsolvation of Cysteine: A Density Functional Theory Study. *J. Phys. Chem. A* **2009**, *113*, 6172–6181.
- (98) Yang, G.; Zhou, L.; Chen, Y. Stabilization of zwitterionic versus canonical proline by water molecules. *SpringerPlus* **2016**, *5*, 19.
- (99) Dohn, A. O. Multiscale electrostatic embedding simulations for modeling structure and dynamics of molecules in solution: A tutorial review. *Int. J. Quantum Chem.* **2020**, *120*, No. e26343.